

Optoelectronic Performance of Radial-Junction Si Nanopillar and Nanohole Solar Cells

Hua-Min Li, *Student Member, IEEE*, Dae-Yeong Lee, *Student Member, IEEE*, and Won Jong Yoo, *Senior Member, IEEE*

Abstract—Two typical radial-junction structures, Si nanopillars (SiNP) and nanoholes, were modeled and compared for solar cell applications. From the physical model using the transport equations, the output performances, e.g., short-circuit current density, open-circuit voltage, energy conversion efficiency, fill factor, etc., were simulated. A maximum efficiency of 21.0% was predicted for Si nanoholes, demonstrating a superior performance of the radial-junction structure compared to SiNPs (14.6%). Also, the dependence of the conversion efficiency on various structural parameters, e.g., substrate thickness, height, feature radius, junction depth, emitter doping concentration, as well as front and back surface recombination velocities, etc., was investigated, providing a design principle for high-efficiency radial-junction solar cells.

Index Terms—Radial junction, Si nanohole (SiNH), Si nanopillar (SiNP), solar cells.

I. INTRODUCTION

PHOTOVOLTAIC (PV) solar energy conversion is considered as a promising approach to achieving green and renewable energy. New PV systems which incorporate optically active nanostructures can offer substantial potential for maximizing the efficiency-cost ratio against traditional fossil fuels [1], [2]. Compared to the conventional planar junction for solar cell applications, radial-junction Si nanostructures, e.g., Si nanowires (SiNWs) [1], [3], Si nanopillars (SiNPs) [4]–[6], Si nanorods [7], etc., have shown their outstanding optical and electrical advantages, such as the following: 1) large junction area due to their 3-D structure; 2) low reflection due to the density-graded surface [8]; 3) high absorption due to the strong diffraction and scattering on the nanostructure surface [9]; 4) long distance in the incident (vertical) direction for optimal light absorption and short distance in the orthogonal (horizontal) direction for effective minority-carrier collection [7], [10]; 5) cost-efficient mass production due to the use of Si raw materials [4], [5]; etc. More recently, Si nanoholes (SiNHs) have been theoretically and experimentally reported

to have a lower mass requirement and a superior efficiency of performance compared to SiNW, planar Si, and pyramid-textured Si solar cells [2], [11], [12], demonstrating that this is a new alternative structure with great potential for cost-efficient PV applications. Although experimental methods to fabricate PV nanostructures are developing rapidly, much less attention has been given to the development of device physics principles that govern the operation of nanostructured solar cells [7]. A physical model for the radial-junction structure is highly required for optoelectronic characterization and structural optimization.

In this paper, a computational model was proposed for the characterization of SiNP and SiNH, which are two typical radial-junction structures with opposite geometry. The feature size and volume filling ratio of both SiNP and SiNH were fixed as identical, in order to provide equal optical properties, e.g., effective refractive index and surface reflectance, for comparative analysis. The simulation starts by solving the transport equations with relative boundary conditions to obtain the output performance characteristics, e.g., short-circuit current density, open-circuit voltage, energy conversion efficiency, fill factor (FF), etc. Efficiencies of 14.6% and 21.0% were predicted for SiNP and SiNH, respectively, where the better optoelectronic performance of SiNH compared to SiNP was interpreted to be due to the enhanced contribution of photocurrent generation from the p-type quasi-neutral region. Finally, the dependence of the conversion efficiency on various structural parameters, e.g., substrate thickness, height, feature radius, junction depth, emitter doping concentration, as well as front and back surface recombination velocities (SRVs), etc., was investigated for both SiNP and SiNH, providing a design principle for high-efficiency radial-junction PV devices.

II. MODELING AND SIMULATION

Fig. 1 shows the modeling of single-radial-junction SiNP and SiNH units, for which the diameter (d), height (H), substrate thickness (t), unit diameter (D), junction depth ($x_n - x'_n$), and base and emitter doping concentrations (N_A and N_D) are set to be identical for comparison. In order to compare the optoelectronic performance, an effective refractive index (n_{eff}) is used to represent and calibrate their optical properties [4]. The effective refractive index n_{eff} is defined as $n_{\text{Si}} - (n_{\text{Si}} - n_{\text{air}})d^2/D^2$ and $n_{\text{air}} + (n_{\text{Si}} - n_{\text{air}})d^2/D^2$ for SiNP and SiNH, respectively, where n_{Si} and n_{air} are the wavelength-dependent refractive indices of Si and air, respectively. At the wavelength

Manuscript received April 27, 2012; accepted June 12, 2012. Date of publication July 18, 2012; date of current version August 17, 2012. This work was supported in part by the Basic Science Research Program through the National Research Foundation of Korea funded by the Ministry of Education, Science, and Technology under Grant 2009-0083540. The review of this paper was arranged by Editor S. Ralph.

The authors are with the Sungkyunkwan University (SKKU) Advanced Institute of Nano Technology, Department of Nano Science and Technology, SKKU, Suwon 440-746, Korea (e-mail: lihuamin@skku.edu; suslick@skku.edu; yoojw@skku.edu).

Color versions of one or more of the figures in this paper are available online at <http://ieeexplore.ieee.org>.

Digital Object Identifier 10.1109/TED.2012.2205000

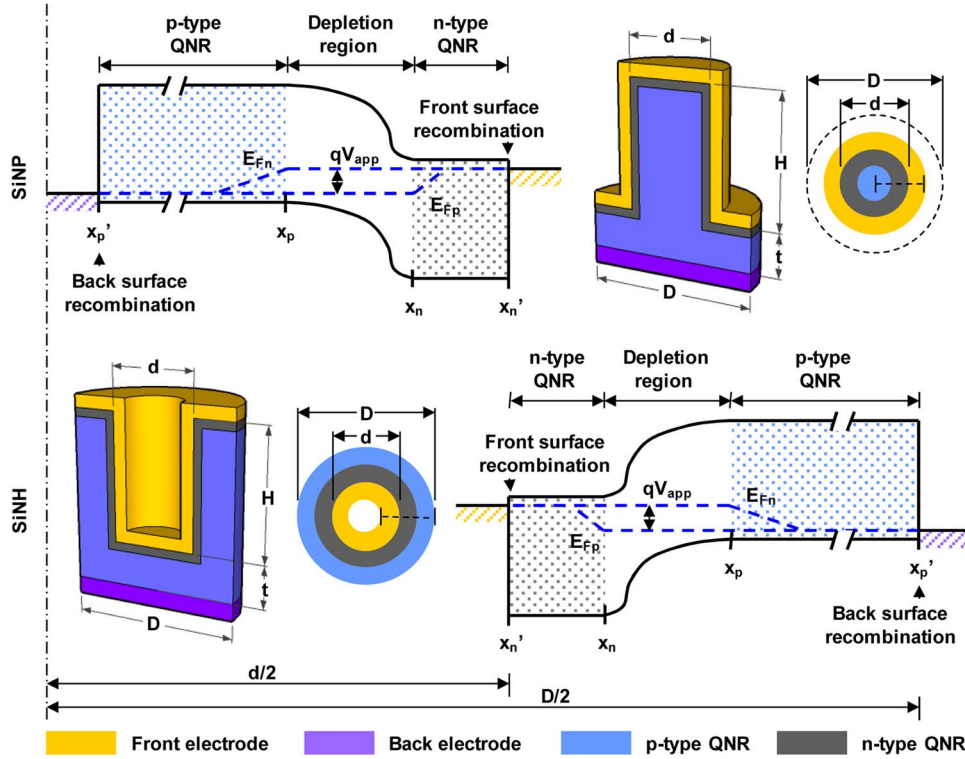


Fig. 1. Schematic of single-radial-junction SiNP and SiNH units and their corresponding energy band diagrams. The structure consists of both planar and radial p-n junctions as well as the front and back electrodes. The p-QNR ($x_p < x < x'_p$), n-QNR ($x'_n < x < x_n$), and depletion region ($x_n < x < x_p$) of the radial junction with front and back surface recombinations at Si-metal interfaces for both SiNP and SiNH structures are illustrated in the energy band diagrams (as denoted by the dash line in the top-view schematics). Here, q , V_{app} , E_{Fn} , and E_{Fp} are the electronic charge, applied voltage (forward biased), and quasi-Fermi-level energies for the electrons and holes, respectively.

of 550 nm, the variation of n_{eff} as a function of the d/D ratio is shown in Fig. 2(a). As the d/D ratio increases, the volume proportions of Si and air in the unit are increased for SiNP and SiNH, respectively, resulting in an increase of n_{eff} for SiNP and a decrease of n_{eff} for SiNH. When the d/D ratio is equal to $1/\sqrt{2}$, both SiNP and SiNH have an identical volume filling ratio [12] of 0.5, a steplike density-graded surface with an intermediate refractive index (n_{eff} of 2.539 at the wavelength of 550 nm) between Si and air, as shown in Fig. 2(b). In this case, the surface optical properties of SiNP and SiNH, e.g., n_{eff} and the surface reflectance as functions of the wavelength, are obtained [13] and compared to those of the flat surface of Si, as shown in Fig. 2(c) and (d). Both SiNP and SiNH have identical optical properties for comparative characterizations, and a suppressed surface reflectance induced by the density-graded structure is observed clearly.

Since the planar junctions in both SiNP and SiNH structures are identical, only the radial junctions are discussed in this work, and their energy band diagrams are shown in Fig. 1. The radial junction is divided into three regions for separate analysis: the quasi-neutral region of the n-type layer (n-QNR) with a width spanning the range between x_n and x'_n , the quasi-neutral region of the p-type layer (p-QNR) with the width between x_p and x'_p , and the depletion region with the width between x_n and x_p . In order to examine the structural effects on the carrier transport, here, we define the QNR as the region between the depletion region and electrodes. Thereby, the holes photon generated at the junction interface would transport horizontally

through the n-QNR and be collected by the front electrode, whereas the electrons would transport vertically through the p-QNR and be collected by the back electrode.

The computational simulation is based on the transport equations which are solved by applying the corresponding boundary conditions with both front and back SRVs [7], [14]. The transport equation for the minority carriers (electrons) in p-QNR is

$$\frac{d^2 n_p}{dx^2} - \frac{n_p - n_{p0}}{D_n \tau_n} = -\frac{\alpha}{D_n} \Gamma \exp[-\alpha(x - x_p)] \quad (1)$$

where n_p and n_{p0} are the nonequilibrium and equilibrium electron densities in the p-layer, respectively. D_n and τ_n are the diffusion coefficient and lifetime of the electron, respectively. α and Γ are the absorption coefficient and photon flux, respectively, as functions of the wavelength ranging from 400 to 1100 nm [14]. The relative boundary conditions for (1) are

$$n_p = n_{p0} \exp\left(\frac{qV_{app}}{k_B T}\right) \text{ at } x = x_p \quad (2)$$

$$(n_p - n_{p0})qS_b = -qD_n \frac{dn_p}{dx} \text{ at } x = x'_p \quad (3)$$

where q is the electronic charge, V_{app} is the applied voltage, k_B is Boltzmann's constant, T is the absolute temperature, and S_b is the back SRV. A solution for n_p that includes contributions from both diffusion and light generation of the minority carrier

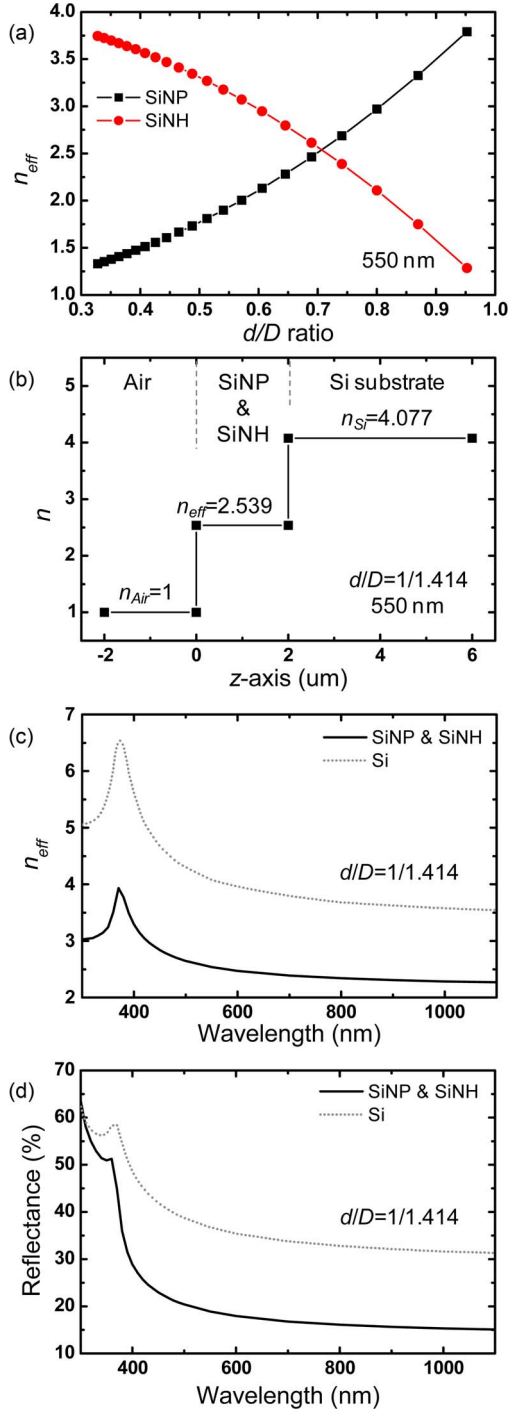


Fig. 2. (a) n_{eff} 's of SiNP and SiNH as functions of the d/D ratio at the wavelength of 550 nm. (b) Refractive index along the z -axis direction at the wavelength of 550 nm, indicating a steplike density-graded surface with an intermediate refractive index. (c) n_{eff} 's of SiNP and SiNH with the d/D ratio of $1/\sqrt{2}$ as functions of the wavelength compared to the flat surface of Si. (d) Surface reflectances of SiNP and SiNH with the d/D ratio of $1/\sqrt{2}$ as functions of the wavelength compared to the flat surface of Si.

is obtained. The effective current density in the p-QNR for the entire radial junction is obtained as

$$J_{\text{p-QNR}} = \frac{2\pi x_p \int_0^H j_{\text{p-QNR}}(z) dz}{\frac{1}{4}\pi D^2} \quad (4)$$

where

$$j_{\text{p-QNR}}(z) = -qD_n \left. \frac{dn_p}{dx} \right|_{x=x_p} \quad (5)$$

is the H -dependent current density in the p-QNR obtained at the depletion edge, $x = x_p$.

The transport equation for the minority carriers (holes) in the n-QNR is

$$\frac{d^2 p_n}{dx^2} - \frac{p_n - p_{n0}}{D_p \tau_p} = -\frac{\alpha}{D_p} \Gamma \exp[-\alpha(x - x'_n)] \quad (6)$$

where p_n and p_{n0} are the nonequilibrium and equilibrium hole densities in the n-layer, respectively. D_p and τ_p are the diffusion coefficient and lifetime of the hole, respectively. The relative boundary conditions for (6) are

$$p_n = p_{n0} \exp\left(\frac{qV_{\text{app}}}{k_B T}\right) \text{ at } x = x_n \quad (7)$$

$$(p_n - p_{n0})qS_f = -qD_p \left. \frac{dp_n}{dx} \right|_{x=x'_n} \quad (8)$$

where S_f is the front SRV. A solution for p_n that includes contributions from both the diffusion and light generation of the minority carrier is obtained. The effective current density in the n-QNR for the entire radial junction is obtained as

$$J_{\text{n-QNR}} = \frac{2\pi x_n \int_0^H j_{\text{n-QNR}}(z) dz}{\frac{1}{4}\pi D^2} \quad (9)$$

where

$$j_{\text{n-QNR}}(z) = qD_p \left. \frac{dp_n}{dx} \right|_{x=x_n} \quad (10)$$

is the H -dependent current density in the n-QNR obtained at the depletion edge, $x = x_n$.

In the depletion region, the photocurrent is approximately equal to the number of photons absorbed per second multiplied by the electronic charge as [14]

$$J_{\text{dep}} = \frac{2\pi (x_p \pm \frac{1}{2}W_{\text{dep}}) \int_0^H j_{\text{dep}}(z) dz}{\frac{1}{4}\pi D^2} \quad (11)$$

where

$$j_{\text{dep}}(z) = q\Gamma \{1 - \exp[-\alpha(x_p - x_n)]\} \quad (12)$$

is the H -dependent current density in the depletion region. The positive and negative signs are used for SiNP and SiNH, respectively, according to their opposite geometries. Assuming that the incident light is normal to the top surface, the photon flux reduces exponentially while penetrating through Si [14], and therefore, the H -dependent current densities, e.g., $j_{\text{p-QNR}}(z)$, $j_{\text{n-QNR}}(z)$, and $j_{\text{dep}}(z)$, are decreased significantly from the top to the bottom of the SiNP and SiNH structures, as shown in Fig. 3(a). The effective current densities, e.g., $J_{\text{p-QNR}}$, $J_{\text{n-QNR}}$, and J_{dep} , for both SiNP and SiNH are obtained via (4), (9), and (11), as shown in Fig. 3(b). A drastic increase in the current density, particularly in $J_{\text{p-QNR}}$, is observed in SiNH compared

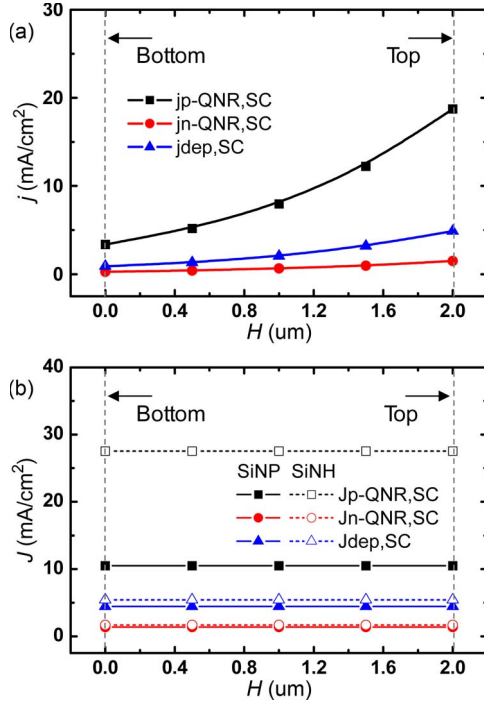


Fig. 3. (a) Variation of H -dependent short-circuit current density ($j_{p-QNR,SC}$, $j_{n-QNR,SC}$, and $j_{dep,SC}$) in the radial junction. (b) Effective short-circuit current density ($J_{p-QNR,SC}$, $J_{n-QNR,SC}$, and $J_{dep,SC}$) in SiNP and SiNH, obtained by integrating the H -dependent current density with the corresponding areas.

to SiNP, owing to its relatively large junction area ($A_j = 2\pi(d/2 + x_n - x'_n)H$). As the A_j increases by increasing the height or reducing the periodicity of the SiNP, SiNH, etc., the photocurrent generation can be enhanced for the constant collecting area ($A_c = 0.25\pi D^2$), giving rise to the increase of photocurrent density which may exceed the theoretical limit for single-junction Si solar cells (43.6 mA/cm²) [15].

The total current for the complete radial junction (J_{sum}) is defined as the sum of the currents from the p-QNR, n-QNR, and depletion region as follows:

$$J_{sum} = J_{p-QNR} + J_{n-QNR} + J_{dep}. \quad (13)$$

Each effective current density and J_{sum} as functions of V_{app} for both SiNP and SiNH are compared, as shown in Fig. 4(a) and (b). The short-circuit J_{p-QNR} ($J_{p-QNR,SC}$), J_{n-QNR} ($J_{n-QNR,SC}$), and J_{dep} ($J_{dep,SC}$) of SiNH are equal to 27.6, 1.7, and 5.4 mA/cm², respectively, which are higher than those of SiNP (10.5, 1.4, and 4.5 mA/cm²). As a result, the short-circuit J_{sum} ($J_{sum,SC}$) and the conversion efficiency (η) of SiNH have the values of 34.6 mA/cm² and 14.5%, respectively, being about 2.0 and 1.8 times higher than those of SiNP (16.9 mA/cm² and 8.0%). By comparing to SiNP, it was found that 96.6% of the increased J_{sum} (17.7 mA/cm²) in SiNH is provided by J_{p-QNR} (17.1 mA/cm²), and this indicates a drastically enhanced contribution of the p-QNR in photocurrent generation. Furthermore, considering the additional contribution from the planar junction (η of 6.6%, FF of 81.2%) and performing the optoelectronic characterizations for the entire unit, total efficiencies of 14.6% and 21.0% are predicted for the SiNP and SiNH units, respectively, as shown in Fig. 4(c) and (d).

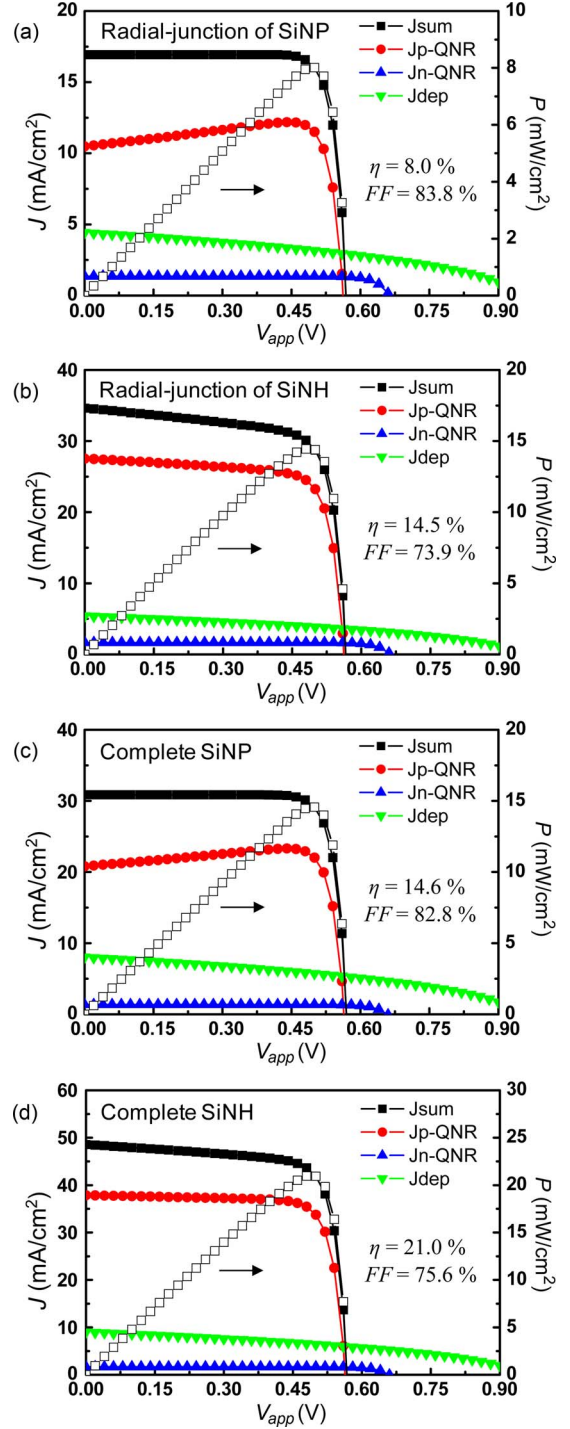


Fig. 4. (a) and (b) J_{sum} (including J_{p-QNR} , J_{n-QNR} , and J_{dep}) and power (P) as functions of V_{app} for the radial junction of SiNP and SiNH, indicating an η value of 8.0% and an FF value of 83.8% for SiNP and an η value of 14.5% and an FF value of 73.9% for SiNH, respectively. (c) and (d) J_{sum} (including J_{p-QNR} , J_{n-QNR} , and J_{dep}) and P as functions of V_{app} for the complete SiNP and SiNH, indicating an η value of 14.6% and an FF value of 82.8% for SiNP and an η value of 21.0% and an FF value of 75.6% for SiNH, respectively. Here, $d = 2 \mu\text{m}$, $H = 2 \mu\text{m}$, $t = 200 \text{ nm}$, $D = 2.828 \mu\text{m}$, $x_n - x'_n = 0.1 \mu\text{m}$, $N_A = 10^{16} \text{ cm}^{-3}$, $N_D = 10^{20} \text{ cm}^{-3}$, $S_f = S_b = 10^4 \text{ cm/s}$, and the surface reflectance is set at 30%.

III. RESULTS AND DISCUSSION

Based on the computational modeling of the radial junction, the dependence of η on various structural parameters, e.g., t , H ,

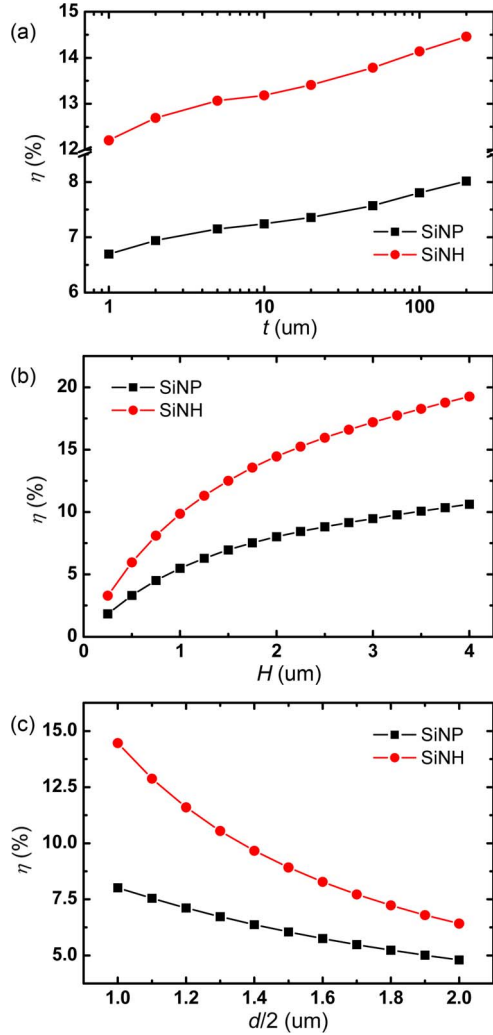


Fig. 5. Dependence of η on (a) t , (b) H , and (c) $d/2$ for both SiNP and SiNH solar cells.

$d/2$, $x_n - x'_n$, N_D , S_f , S_b , etc., are examined comprehensively, providing a design principle for realizing high-efficiency radial-junction SiNP and SiNH PV devices.

- 1) Substrate thickness (t). In the radial junction, only $J_{\text{p-QNR}}$ varies with t due to the t -dependent width of p-QNR, which is defined as the region between the depletion layer and the back electrode. As t increases, from 2 (the thin-film devices) to 200 μm (the wafer-based devices), $J_{\text{p-QNR}}$ and, thereby, J_{sum} are increased due to enhanced photon absorption in the extended p-QNR, giving rise to an increase of η , as shown in Fig. 5(a).
- 2) Height (H). The increase of H relatively extends the p-QNR and enhances the photon absorption in the incident direction, resulting in an improved photocurrent generation, as shown in Fig. 5(b). However, η starts to saturate as $H > 2 \mu\text{m}$ since 81.9% of the photons are absorbed within 2 μm in the exponential manner. Therefore, $\sim 2 \mu\text{m}$ is considered to be the optimized height for the radial-junction structure.
- 3) Feature radius ($d/2$). The increase of $d/2$ enlarges A_j and enhances the photocurrent generation for a single unit, but it also reduces the unit density and, then, the total pho-

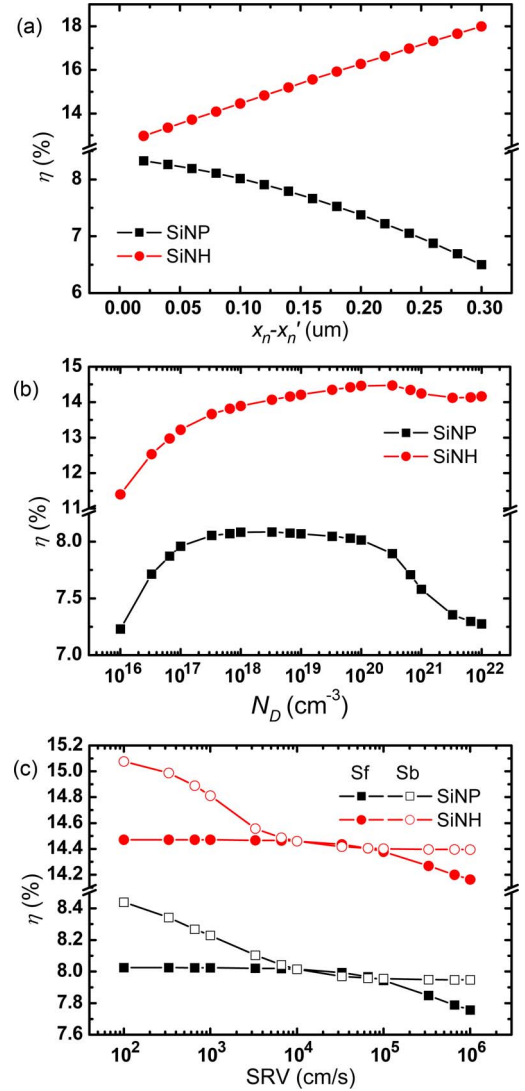











Fig. 6. Dependence of η on (a) $x_n - x'_n$, (b) N_D , and (c) S_f and S_b for both SiNP and SiNH solar cells.

tocurrent generation for a multiunit system. Therefore, the D -dependent A_c is used to represent the effect of the array periodicity. According to (4), (9), and (11), as $d/2$ increases for the constant d/D ratio of $1/\sqrt{2}$, the increase of D -dependent A_c is faster than that of d -dependent A_j , resulting in a degraded photocurrent generation, as shown in Fig. 5(c).

- 4) Junction depth ($x_n - x'_n$). $x_n - x'_n$ directly affects the width of n-QNR and A_j . As it increases from 0.02 to 0.3 μm for SiNP, A_j shrinks significantly from 12.31 to 8.80 μm^2 , resulting in a reduction of photocurrent generation, as shown in Fig. 6(a). However, as it increases for SiNH, A_j is extended from 12.82 to 16.34 μm^2 , giving rise to an enhanced photocurrent generation. Meanwhile, $J_{\text{n-QNR}}$ is increased with increasing $x_n - x'_n$ since more photons can be absorbed in the extended n-QNR, although the extension of the n-QNR degrades the carrier collection due to the increased transport distance [5].
- 5) Emitter doping concentration (N_D). The surface texture inevitably enhances the front surface recombination due

TABLE I
COMPARISON OF OPTOELECTRONIC PERFORMANCE AMONG RADIAL-JUNCTION SiNP AND SiNH AND THE OTHER TYPES OF SURFACE TEXTURED SOLAR CELLS. ¹THOSE RESULTS WERE OBTAINED VIA THE EXPERIMENTS IN WHICH VARIOUS TECHNIQUES, E.G., ANTIREFLECTION COATING, BURIED TOP CONTACT, ETC., WERE ALSO INCLUDED

| Types Parameter | This work: SiNP (radial-junc.) | This work: SiNH (radial-junc.) | Si planar cell [7] | Si pyramidal cell [17] (upright) ¹ | Si pyramidal cell [18] (inverted) ¹ | Si nanocone (SiNC) [4] | SiNW [19] (subsurface- junc.) | SiNW [4] (planar-junc.) | SiNW [7] (radial-junc.) |
|--------------------------------|---|---|---|---|---|---|---|---|---|
| Schematic of single unit |  |  |  |  |  |  |  |  |  |
| J_{sc} (mA/cm ²) | 30.8 | 48.6 | ~35 | 36.9 | 40.9 | / | / | / | ~43 |
| V_{oc} (V) | 0.57 | 0.57 | ~0.6 | 0.60 | 0.71 | / | 0.55 | / | ~0.52 |
| η (%) | 14.6 | 21.0 | ~18 | 16.7 | 24.0 | ~22.5 | ~9.3 | ~17.5 | ~17 |
| FF (%) | 82.8 | 75.6 | / | 75.2 | 82.7 | / | 65 | / | / |

to the enlarged surface area and consequently induces a degradation of η . Increasing N_D is one solution for suppressing the surface recombination due to the reduction of the minority-carrier concentration [4], [5]. However, the carrier collection is also reduced for high N_D due to the degradation of carrier mobility (μ_p), lifetime (τ_p), diffusion coefficient (D_p), length (L_p), etc. [16]. These parameters and N_D synthetically affect the complete optoelectronic performance of SiNP and SiNH solar cells. As a result of the tradeoff between these two competing mechanisms, the maximum efficiency is obtained when N_D is equal to $\sim 10^{18}$ and $\sim 10^{20}$ cm⁻³ for SiNP and SiNH, respectively, as shown in Fig. 6(b).

- 6) SRV. The dependence of η on both S_f and S_b is analyzed by examining a wide range of SRV from 10^2 to 10^6 cm/s, as shown in Fig. 6(c). It is found that the drastic degradation of η in a radial-junction structure occurs at high S_f (over 10^4 cm/s) or low S_b (below 10^4 cm/s). This can be interpreted as being the result of the different contributions of the p-QNR and n-QNR to the photocurrent generation. For example, J_{n-QNR} , which is affected by S_f , contributes only a small proportion of J_{sum} (see Fig. 3) due to its relatively low minority-carrier concentration, so its influence on η is not obvious in the low S_f range but appears in the high S_f range where the reduction of the current generation is no longer negligible. As a comparison, J_{p-QNR} , which is affected by S_b , contributes greatly to the complete photocurrent generation (see Fig. 3) due to its relatively high minority-carrier concentration. A small increase of S_b would induce a drastic reduction of J_{p-QNR} , resulting in the degradation of J_{sum} and η .

In summary, the optoelectronic performances of the radial-junction SiNP and SiNH solar cells are compared to the other types of surface textured devices, such as the planar cell [7], pyramidal cell [17], [18], Si nanocone [4], SiNW [4], [7], [19], etc., as listed in Table I.

IV. CONCLUSION

In this paper, the physical modeling of both radial-junction SiNP and SiNH has been performed, and their optoelectronic properties have been comparatively investigated. Efficiencies of 14.6% and 21.0% have been predicted for SiNP and SiNH, respectively, indicating the superior performance of the radial-

junction SiNH surface textures. The dependence of the efficiency on various structural parameters has been investigated, providing a guideline for the design and optimization of high-efficiency PV devices.

REFERENCES

- [1] B. Tian, X. Zheng, T. J. Kempa, Y. Fang, N. Yu, G. Yu, J. Huang, and C. M. Lieber, "Coaxial silicon nanowires as solar cells and nanoelectronic power sources," *Nature*, vol. 449, no. 7164, pp. 885–889, Oct. 2007.
- [2] K.-Q. Peng, X. Wang, L. Li, X.-L. Wu, and S.-T. Lee, "High-performance silicon nanohole solar cells," *J. Amer. Chem. Soc.*, vol. 132, no. 20, pp. 6872–6873, May 2010.
- [3] Z. W. Pei, S. T. Chang, C. W. Liu, and Y. C. Chen, "Numerical simulation on the photovoltaic behavior of an amorphous-silicon nanowire-array solar cell," *IEEE Electron Device Lett.*, vol. 30, no. 12, pp. 1305–1307, Dec. 2009.
- [4] J. S. Li, H. Y. Yu, S. M. Wong, G. Zhang, X. W. Sun, G. Q. Lo, and D. L. Kwong, "Surface nanostructure optimization for solar energy harvesting in Si thin film based solar cells," in *IEDM Tech. Dig.*, 2009, pp. 547–550.
- [5] S. M. Wong, H. Y. Yu, J. S. Li, G. Zhang, P. G. Q. Lo, and D. L. Kwong, "Design high-efficiency Si nanopillar-array-textured thin-film solar cell," *IEEE Electron Device Lett.*, vol. 31, no. 4, pp. 335–337, Apr. 2010.
- [6] J. S. Li, H. Y. Yu, S. M. Wong, G. Zhang, X. W. Sun, P. G. Q. Lo, and D. L. Kwong, "Si nanopillar array optimization on Si thin films for solar energy harvesting," *Appl. Phys. Lett.*, vol. 95, no. 3, p. 033102, Jul. 2009.
- [7] B. M. Kayes, H. A. Atwater, and N. S. Lewis, "Comparison of the device physics properties of planar and radial p-n junction nanorod solar cells," *J. Appl. Phys.*, vol. 97, no. 11, p. 114302, May 2005.
- [8] H. C. Yuan, V. E. Yost, M. R. Page, P. Stradins, D. L. Meier, and H. M. Branz, "Efficient black silicon solar cell with a density-graded nanoporous surface: Optical properties, performance limitations, and design rules," *Appl. Phys. Lett.*, vol. 95, no. 12, p. 123501, Sep. 2009.
- [9] R. A. Street, P. Qi, R. Lujan, and W. S. Wong, "Reflectivity of disordered silicon nanowires," *Appl. Phys. Lett.*, vol. 93, no. 16, p. 163109, Oct. 2008.
- [10] M. D. Kelzenberg, D. B. Turner-Evans, B. M. Kayes, M. A. Filler, M. C. Putnam, N. S. Lewis, and H. A. Atwater, "Photovoltaic measurements in single-nanowire silicon solar cells," *Nano Lett.*, vol. 8, no. 2, pp. 710–714, Feb. 2008.
- [11] F. Wang, H. Y. Yu, J. S. Li, X. W. Sun, X. C. Wang, and H. Y. Zheng, "Optical absorption enhancement in nanopore textured-silicon thin film for photovoltaic application," *Opt. Lett.*, vol. 35, no. 1, pp. 40–42, Jan. 2010.
- [12] S. E. Han and G. Chen, "Optical absorption enhancement in silicon nanohole arrays for solar photovoltaics," *Nano Lett.*, vol. 10, no. 3, pp. 1012–1015, Feb. 2010.
- [13] *The Optical Properties Were Obtained via Luxpop Thin Film and Bulk Index of Refraction and Photonics Calculations*. [Online]. Available: www.luxpop.com
- [14] A. L. Fahrenbruch and R. H. Bube, *Fundamentals of Solar Cells: Photovoltaic Solar Energy Conversion*. New York: Academic, 1983.
- [15] F. Meillaud, A. Shah, C. Droz, E. Vallat-Sauvain, and C. Miazza, "Efficiency limits for single-junction and tandem solar cells," *Solar Energy Mater. Sol. Cells*, vol. 90, no. 18/19, pp. 2952–2959, Nov. 2006.

- [16] Y. Taur and T. H. Ning, *Fundamentals of Modern VLSI Devices*. New York: Cambridge Univ. Press, 1998.
- [17] J. C. Zolper, S. Narayanan, S. R. Wenham, and M. A. Green, "16.7% efficient, laser textured, buried contact polycrystalline silicon solar cell," *Appl. Phys. Lett.*, vol. 55, no. 22, pp. 2363–2365, Nov. 1989.
- [18] J. Zhao, A. Wang, P. Altermatt, and M. A. Green, "Twenty-four percent efficient silicon solar cells with double layer antireflection coatings and reduced resistance loss," *Appl. Phys. Lett.*, vol. 66, pp. 3636–3638, Jun. 1995.
- [19] K.-Q. Peng and S.-T. Lee, "Silicon nanowires for photovoltaic solar energy conversion," *Adv. Mater.*, vol. 23, no. 2, pp. 198–215, Jan. 2010.



Dae-Yeong Lee (S'11) received the M.S. degree from Sungkyunkwan University (SKKU), Seoul, Korea, in 2012, where he is currently working toward the Ph.D. degree in the SKKU Advanced Institute of Nano Technology.



Hua-Min Li (S'11) received the M.S. degree from the College of Engineering, Sungkyunkwan University (SKKU), Seoul, Korea, in 2010, where he is currently working toward the Ph.D. degree in the SKKU Advanced Institute of Nano Technology.



Won Jong Yoo (M'00–SM'02) received the Ph.D. degree from Rensselaer Polytechnic Institute, Troy, NY.

He is with the Sungkyunkwan University (SKKU) Advanced Institute of Nano Technology, Department of Nano Science and Technology, SKKU, Seoul, Korea.